Analyst

ROYAL SOCIETY OF CHEMISTRY

PAPER

View Article Online
View Journal | View Issue

Cite this: *Analyst*, 2024, **149**, 2709

Nutrient supplementation-induced metabolic profile changes and early appearance of free *N*-glycans in nutrient deficient tomato plants revealed by mass spectrometry

Marjan Dolatmoradi,[a] Zsolt Sándor,[b] Imre Vágó,[b] Daniel A. Lowy,[c] Akos Vertes *[a] and Ida Kincses*[b]

Inorganic fertilizers are routinely used in large scale crop production for the supplementation of nitrogen, phosphorus, and potassium in nutrient poor soil. To explore metabolic changes in tomato plants grown on humic sand under different nutritional conditions, matrix-assisted laser desorption ionization (MALDI) mass spectrometry was utilized for the analysis of xylem sap. Variations in the abundances of metabolites and oligosaccharides, including free *N*-glycans (FNGs), were determined. Statistical analysis of the sample-related peaks revealed significant differences in the abundance ratios of multiple metabolites, including oligosaccharides, between the control plants, grown with no fertilizers, and plants raised under "ideal" and "nitrogen deficient" nutritional conditions, *i.e.*, under the three treatment types. Among the 36 spectral features tentatively identified as oligosaccharides, the potential molecular structures for 18 species were predicted based on their accurate masses and isotope distribution patterns. To find the spectral features that account for most of the differences between the spectra corresponding to the three different treatments, multivariate statistical analysis was carried out by orthogonal partial least squares-discriminant analysis (OPLS-DA). They included both FNGs and non-FNG compounds that can be considered as early indicators of nutrient deficiency. Our results reveal that the potential nutrient deficiency indicators can be expanded to other metabolites beyond FNGs. The *m*/*z* values for 20 spectral features with the highest variable influence on projection (VIP) scores were ranked in the order of their influence on the statistical model.

Received 4th January 2024,
Accepted 18th March 2024

DOI: 10.1039/d4an00024b

rsc.li/analyst

Introduction

Applying appropriate levels of nitrogen fertilizers can improve the carbohydrate and organic acid metabolism in young tomato plants.[1] However, overfertilization can result in the generation of reactive oxygen species that can cause extensive cellular damage and make plants more prone to attack by pests and pathogens.[2,3] Therefore, it is desirable to find biomarkers that signal the need for nutritional supplementation under specific growth conditions. Early detection of nutrient deficiencies and subsequent supplementation are essential, as their absence can significantly reduce yields and thus economic returns.[4] Previous studies on *Arabidopsis thaliana* grown under nitrogen deficient conditions have demonstrated a significant decrease in the levels of most amino acids, organic acids involved in the tricarboxylic cycle, and other N-containing species, such as chlorophyll.[3,5] The effect of biological nitrogen fixation on xylem sap metabolite composition was also studied in soybean (*Glycine max*) by comparing plants infected with rhizobia (*Bradyrhizobium japonicum*) and uninfected plants. Nitrogen containing compounds, *e.g.*, allantoin, allantoic acid, hydroxymethylglutamate, and methylene glutamate, were found to be more abundant in the presence of nitrogen fixation.[6] However, due to the large number of metabolic pathways and the complex interconnectivity between them, predicting their response to nutrient deficiency and supplementation requires extensive information on metabolite pool sizes and *in vivo* reaction rates.

Non-conjugated N-type oligosaccharides designated as free *N*-glycans (FNGs) are signaling molecules involved in various biological processes that exist at micromolar concentrations in plant cells.[7,8] They can be produced in the endoplasmic reticulum and/or the Golgi apparatus within a cell.[9] They interact with cell surface receptors and other proteins, affecting cell be-

[a]*Department of Chemistry, George Washington University, Washington, DC, USA. E-mail: vertes@gwu.edu*
[b]*Faculty of Agricultural and Food Sciences and Environmental Management, University of Debrecen, Hungary. E-mail: kincsesi@agr.unideb.hu*
[c]*Hungarian Innovation Agency, Budapest, Hungary*

havior and communication. Protein-linked *N*-glycans facilitate the quality control of protein folding in the endoplasmic reticulum and play an essential role in cellular response to environmental perturbations.[10] Changes in glycans composition can result from elevated levels of stress hormones (*e.g.*, ethylene, jasmonic acid, *etc.*) under nutrient-deficient conditions that stimulate several mechanisms including the induction of glycosyltransferases in plants.[11]

FNGs can be found in different plant tissues including leaves, roots, and developing fruits.[8] Their types and abundances can reflect changes in protein glycosylation, cell wall composition, and signaling pathways in response to environmental stressors like pathogens, or temperature variations.[12] Recent studies have begun to unravel the specific role of FNGs in developing tomato plants. They are shown to be associated with fruit ripening and seed development.[13,14] Gaining insight into the biological function of these molecules in response to stress allows the development of strategies to improve plant resilience and crop yield under adverse conditions. Their early detection in plant life can also signal nutritional and climate change-related challenges to plant health.

FNGs can be classified as high mannose type (GN1) and plant complex type (GN2), built from GlcNAc, and GlcNAcβ1-4GlcNAc residues at the reducing end, respectively. These forms of FNGs are released from glycoproteins through the action of glycanases, including *endo*-*N*-acetyl-β-D-glucosaminidase (ENGase), which gives rise to GN1 type and peptide-*N*4-(*N*-acetyl-β-D-glucosaminyl) asparagine amidase (PNGase) resulting in GN2 type FNGs.[12] ENGase, in particular, has a significant impact on the ripening process of tomato (*Solanum lycopersicum*) fruits.[15] Recent research has indicated a statistical correlation between nutritional state and the FNG profiles captured by capillary electrophoresis in the xylem sap of tomato plants.[11,16]

In this work, the utility of matrix-assisted laser desorption ionization mass spectrometry (MALDI-MS) is explored for the detection of metabolic profile changes and the typing of FNGs in tomato xylem sap. Sap samples from plants grown under three different treatments are analyzed by a high-performance mass spectrometer. Tentative peak annotations are offered based on highly accurate *m*/*z* values, isotope distribution patterns, and database searches.

Methods

Plants, soil, nutritional conditions, and sampling

Tomato (*S. lycopersicum* var. 'Roma VF') seeds were planted in culture pots containing humus sand from the Pallag Experimental Station of Horticulture (47° 35′ 23″ North, 21° 38′ 18″ East) at the University of Debrecen, located in the Northern Great Plain Region of Hungary. Then, the tomato plants were raised in a greenhouse of the Institute of Agricultural Chemistry and Soil Sciences at the University of Debrecen. Daytime temperatures were between 21 and 26 °C, whereas during the night 16 to 18 °C temperatures were observed. The soil had an Arany plasticity index, K_A, value of 30, consistent with humus sand. Speciation methods for the chemical composition of the soil had been reported earlier.[17] Briefly, the ammonium lactate (AL) soluble components of the soil were extracted with a mixture of 0.1 M AL and 0.4 M acetic acid at pH = 3.7. The extract represented the readily soluble components and some of the reserves of the soil. The calcium chloride soluble components were extracted with aqueous 0.01 M $CaCl_2$ solution. The extract corresponded to the soluble components that can be easily absorbed by the plants. Soil pH was determined after mixing the samples with 1 M KCl solution in 1.0/2.5 ratio (w/w). The most relevant physical and chemical properties of the soil are summarized in Table 1.

The culture pots were weighed daily and watered from the top with distilled water to reach 50% of the water holding capacity of the soil found in the field. The plants were growing at ambient temperatures and light conditions. To determine the outlay of N, P, and K for nutrient supplementation, we relied on the plant-accessible components in the soil, and the specific nutrient requirements of tomatoes in field production. The latter is estimated at 2.7 kg, 2.3 kg, and 4.8 kg of N, P_2O_5, and K_2O, respectively, per metric ton of tomatoes. Nitrogen and phosphorous were added as $NH_4H_2PO_4$ and NH_4NO_3 solutions, whereas potassium was supplied as KCl solution.

Experiments were conducted in nine culture pots with two plants in each pot. Each pot contained 3.0 kg air dry soil. Tomato seedlings emerged seven days after the seeds were planted. They were raised under three different nutritional conditions. Compared to the Control (T1) with no nutritional supplementation, T2 represented the "ideal" nutrition with the addition of N, P, and K at 0.196 g per pot, 0.0712 g per pot, and 0.27 g per pot, respectively, in 20 mL per pot of the nutrient solutions at the beginning of the experiment. Nitrogen-deficient growth conditions (T3) were created by supplement-

Table 1 Physical properties and chemical composition of humus sand of Pallag used as control (T1).[17]

K_A (Arany plasticity index)	30
pH (in 1 M KCl)	5.76
Humus content	1.57%
Total water-soluble salts	0.02% (w/w)
Species soluble in AL[22]	**(mg kg^{-1})**
P_2O_5	205.6
K_2O	254.8
Ca	1089
Mg	160.3
Mn	105.1
Zn	2.64
Cu	5.81
Na	58.6
Species soluble in 1 M KCl	**(mg kg^{-1})**
NO_3	12.3
Mg	157
S	6.43
Species soluble in 0.01 M $CaCl_2$[23,24]	**(mg kg^{-1})**
Total N	25.04
N as NO_3	13.53
N as NH_3	6.8
N as organic species	4.71

Table 2 Nutritional conditions for tomato plants under three treatments

Treatment	Nutritional conditions	Sample designations
T1	Control	S1, S6, S11
T2	N, P, and K supplemented ("Ideal")	S2, S7, S12
T3	N deficient, P and K supplemented	S3, S8, S13

ing 0.0712 g per pot and 0.27 g per pot of P and K, respectively, in 20 mL per pot of the nutrient solutions, whereas only 0.098 g per pot of N in 20 mL solution was added at the beginning of the experiment.

Xylem sap of 61-day-old plants was collected according to the protocol described by Tsujimori *et al.*[18] stored at −80 °C and lyophilized. Table 2 shows the grouping of samples according to treatment, *i.e.*, according to the nutritional conditions.

Mass spectrometry

For the analysis of tomato sap by MALDI-MS, 1 mg of the lyophilized samples from treatments T1, T2, and T3 were resuspended in 500 μL of HPLC-grade water (W5-4, Fisher Scientific, Waltham, MA, USA) and agitated for 15 min. The resuspended lyophilate was then centrifuged at 11 000 rpm for 20 min (Centrifuge 5430 R, Eppendorf AG, Hamburg, Germany). The supernatants were collected and mixed in a 2 : 5 volume ratio with 10 mg mL^{-1} of MALDI matrix dissolved in methanol (A452-4, Fisher Scientific, Waltham, MA, USA). The tested matrices were α-cyano-4-hydroxycinnamic acid (CHCA, catalog no. C8982) and 2,5-dihydroxybenzoic acid (DHB, catalog no. 58707) purchased from Sigma Aldrich (St Louis, MO, USA). A well-controlled sample preparation process, including efficient free glycan recovery and homogenized matrix-supernatant mixture production, was implemented to support reproducibility. Signal reproducibility was evaluated by using analytical replicates for each treatment. For analysis, 1.5 μL of the resulting matrix-supernatant mixture was deposited onto a stainless-steel sample plate and left to dry in air at ambient temperature. Mass spectra were collected by a MALDI-LTQ-Orbitrap XL MS (Thermo Scientific, San Jose, CA, USA) with the acquisition range set to *m*/*z* 150 to 2000. A resolving power of 30 000 was maintained in all measurements. Ions were generated by pulses from a nitrogen laser emitting at 337 nm with a 60 Hz repetition rate and focused on the sample surface resulting in a fluence of 16 mJ cm^{-2} with 10 shots per scan. Regular instrument calibration, using a ProteoMass MALDI Calibration Kit (MSCAL4, Sigma-Aldrich, St Louise, MO, USA), ensured consistent *m*/*z* measurements over time.

After the acquisition, raw data files (*.raw) were imported into the Xcalibur software (Thermo Scientific, San Jose, CA, USA) for processing. Averaged mass spectra were uploaded into mMass for peak picking (S/N > 3) and deisotoping. Accurate masses and isotope distribution patterns were used for tentative ion annotations. The GlycoMod tool at the Expasy portal (**https://web.expasy.org/glycomod/**, last visited 10/5/2023), was designed to predict oligosaccharide structures, including *N*-glycans. It was used for tentative peak annotations.[19] The

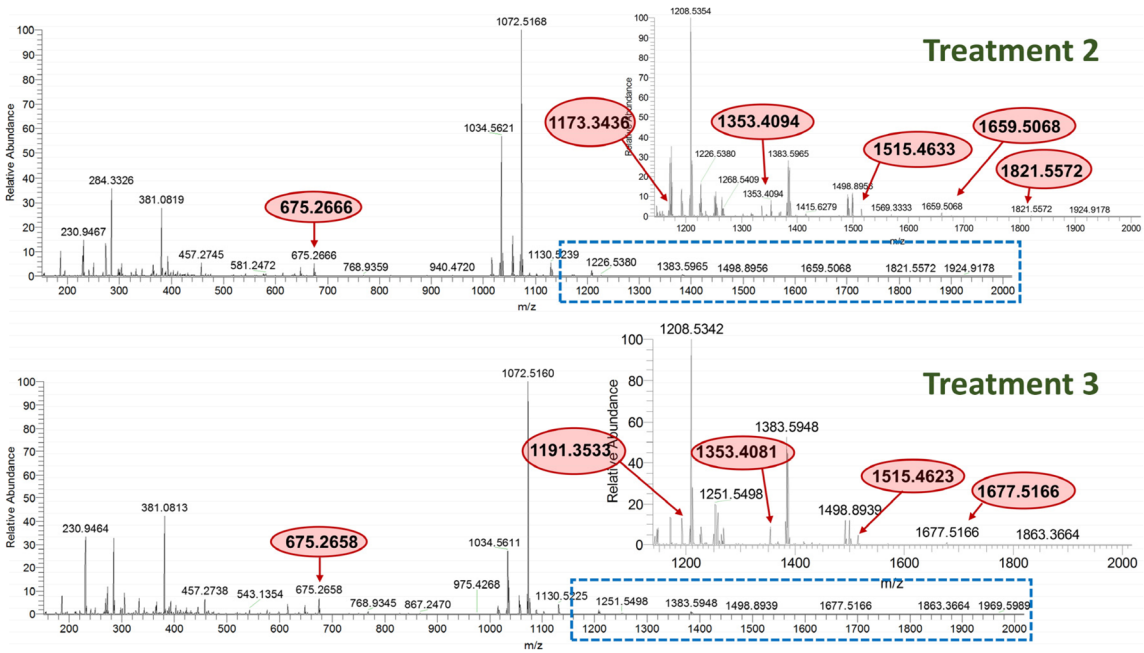

Fig. 1 MALDI mass spectra of samples B7 (top panel) and B3 (bottom panel), associated with treatments T2 (N, P, and K supplementation) and T3 (P and K supplementation), respectively. The samples were mixed with DHB matrix and analyzed in positive ion mode. Peaks tentatively assigned to FNGs are circled in red.

m/z values for spectral features of interest were entered into GlycoMod and potential structures were explored with a Δm = ±20 mDa mass tolerance. Some searches resulted in multiple structures belonging to quasi-isobaric ions and/or structural isomers.

To identify the significantly regulated spectral features, statistical analysis was performed using MetaboAnalyst (**https://www.metaboanalyst.ca/MetaboAnalyst/**, last visited 10/5/2023). Peak intensities were normalized by the sum of sample-related ion abundances, log-transformed, and subjected to Pareto scaling. To identify biomarker candidates, univariate (volcano plot) and multivariate (orthogonal partial least squares-discriminant analysis (OPLS-DA)) methods were used on the normalized data. Datasets included 804, 664, and 747 spectral features for T1, T2, and T3, respectively, for the DHB matrix, and 1058, 986, and 953 spectral features for T1, T2, and T3, respectively, for the CHCA matrix.

To identify biologically and statistically significant spectral features, volcano plots were created with fold change (FC > 2) and *p*-value ($p < 0.05$) thresholds, respectively. Using OPLS-DA, potential biomarkers, responsible for most of the variance between spectra from different treatments, *i.e.*, spectral features with high correlation and covariance, were found from *S*-plots. The most influential spectral features in the separation of treatment groups were also characterized by the variable influence on projection (VIP) scores.

Results and discussion

Two examples of MALDI mass spectra (DHB matrix and positive ion mode) obtained from the analysis of tomato sap samples B7 and B3 for treatments T2 and T3, respectively, are displayed in Fig. 1. Some of the peaks tentatively assigned as FNGs are highlighted in each spectrum. A partial list of potential structures is shown in Table 3. The potential structures of oligosaccharides within the mass tolerance window were predicted using the GlycoMod tool. As revealed by Fig. 1, there are several common spectral features present for the two treatments (*e.g.*, *m/z* 675.266, *m/z* 1353.408, and *m/z* 1515.462), whereas some other oligosaccharides exhibit differences in their absolute ion intensities. For example, the peak at *m/z* 1173.344 demonstrated high and low intensities ($FC_{T2/T3} \approx 1.8$) for T2 and T3 samples, respectively, whereas the peak detected

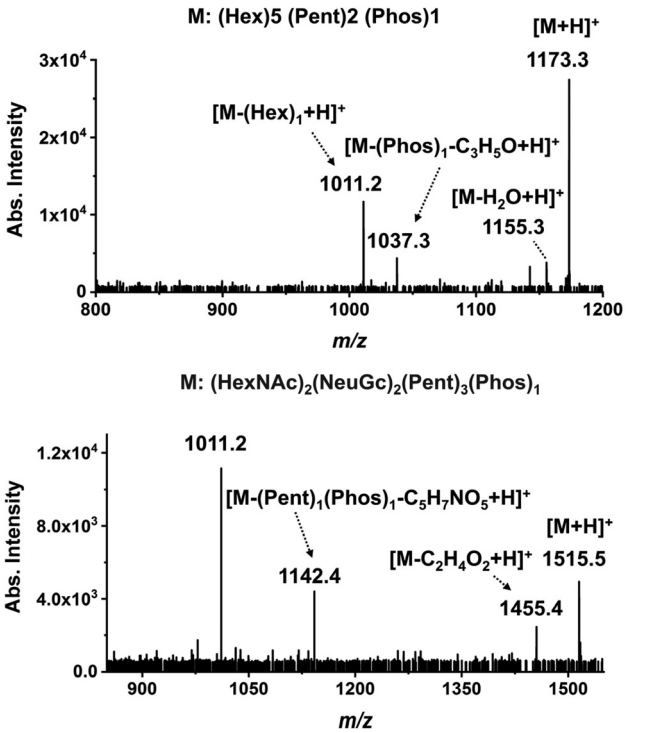

Fig. 2 Tandem MS at 40 eV collision energy for precursor ions *m/z* 1173.337 (top panel) and *m/z* 1515.462 (bottom panel). Compositions of the corresponding molecules (M) are shown above the spectra.

Table 3 Structures of free non-conjugated oligosaccharides tentatively assigned to selected *m/z* values and their ion abundances, I, (in 1000 counts) for treatments T1, T2, and T3

m/z	Adduct	Glycoform mass	Δm (mDa)	Structure	I(T1)	I(T2)	I(T3)
222.091	$[M + H]^+$	203.079	−4	$(HexNAc)_1$	600	590	580
475.156	$[M + H]^+$	456.148	−9	$(Hex)_2$ $(Pent)_1$	48	120	170
649.119	$[M + H]^+$	630.096	5	$(Hex)_2$ $(Deoxyhexose)_1$ $(Phos)_2$	23	19	28
657.168	$[M + H]^+$	638.146	4	$(Hex)_1$ $(Pent)_3$ $(Phos)_1$	11	9	9
675.266	$[M + H]^+$	656.228	20	$(Hex)_1$ $(HexNAc)_1$ $(NeuAc)_1$	1093	1272	982
849.231	$[M + H]^+$	830.209	4	$(Hex)_3$ $(Pent)_2$ $(Phos)_1$	11	4	7
1173.337	$[M + H]^+$	1154.315	4	$(Hex)_5$ $(Pent)_2$ $(Phos)_1$	56	9	5
1175.352	$[M + H]^+$	1156.332	2	$(HexNAc)_1$ $(NeuAc)_3$ $(Phos)_1$	3	—	—
1021.267	$[M + H]^+$	1002.248	1	$(Hex)_2$ $(NeuAc)_1$ $(NeuGc)_1$ $(Sulph)_1$	4	4	1
1191.348	$[M + H]^+$	1172.327	4	$(HexNAc)_1$ $(NeuAc)_2$ $(NeuGc)_1$ $(Phos)_1$	42	41	75
1317.414	$[M + H]^+$	1298.394	2	$(Hex)_4$ $(Deoxyhexose)_3$ $(Pent)_1$ $(Phos)_1$	—	14	2
1353.408	$[M + H]^+$	1334.38	10	$(Hex)_1$ $(HexNAc)_1$ $(NeuAc)_2$ $(NeuGc)_1$ $(Phos)_1$	28	46	80
1515.462	$[M + H]^+$	1496.433	11	$(HexNAc)_2$ $(NeuGc)_2$ $(Pent)_3$ $(Phos)_1$	41	20	37
1659.507	$[M + H]^+$	1640.502	−12	$(Hex)_1$ $(HexNAc)_2$ $(Deoxyhexose)_1$ $(NeuAc)_2$ $(Pent)_2$ $(Sulph)_1$	12	8	11
1677.517	$[M + H]^+$	1658.485	14	$(Hex)_1$ $(HexNAc)_2$ $(NeuGc)_2$ $(Pent)_3$ $(Phos)_1$	31	5	22
1821.557	$[M + H]^+$	1802.548	−8	$(HexNAc)_6$ $(Deoxyhexose)_2$ $(Pent)_1$ $(Sulph)_2$	3	3	3
1828.687	$[M + H]^+$	1809.666	4	$(Hex)_1$ $(HexNAc)_3$ $(Deoxyhexose)_1$ + $(Man)_3(GlcNAc)_2$	9	—	—
1842.653	$[M + H]^+$	1823.645	−9	$(HexNAc)_1$ $(Deoxyhexose)_1$ $(NeuAc)_2$ + $(Man)_3(GlcNAc)_2$	8	—	—

at m/z 1191.353 showed an opposite variation ($FC_{T2/T3} \approx 0.55$) in ion abundances. Among the species listed in Table 3, potential structures belonging to m/z 1828.687 and m/z 1842.653 were found to be FNGs. A previous study has documented that predominantly GN2-type FNGs exist in tomato xylem sap.[18]

Analyzing the samples using the two matrices (DHB and CHCA) resulted in improved molecular coverage. Although the total number for the peaks of interest was higher with the DHB matrix, using CHCA enabled the detection of a few additional N-linked oligosaccharides (*e.g.*, species at m/z 222.091 and m/z 1569.340). A total of 36 spectral features, tentatively identified as oligosaccharides (including FNGs), were detected in the samples (34 and 18 using DHB and CHCA, respectively). To confirm the peak annotation, tandem mass spectra at 40 eV collision energy for two species at the m/z 1173.337 and m/z 1515.462 identified as $(Hex)_5(Pent)_2(Phos)_1$ and $(HexNAc)_2(NeuGc)_2(Pent)_3(Phos)_1$ are shown in Fig. 2.

Once all sample-related peaks were extracted, a filtering process was implemented to identify the list of potentially interesting features. A commonly used filtering tool is the

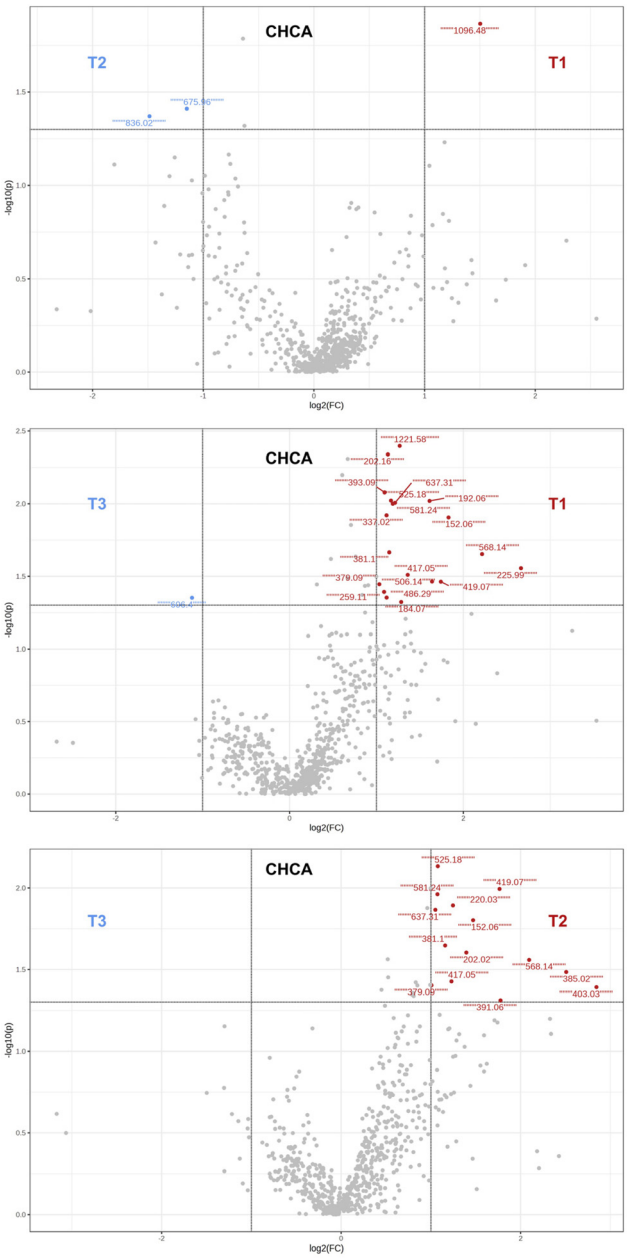

Fig. 3 Volcano plots show significantly up- and downregulated spectral features (CHCA matrix) for treatment comparisons T1 *vs.* T2 (top panel), T1 *vs.* T3 (middle panel), and T2 *vs.* T3 (bottom panel). A total of 3, 20, and 14 regulated species were found for T1 *vs.* T2, T1 *vs.* T3, and T2 *vs.* T3 treatment pairs, respectively.

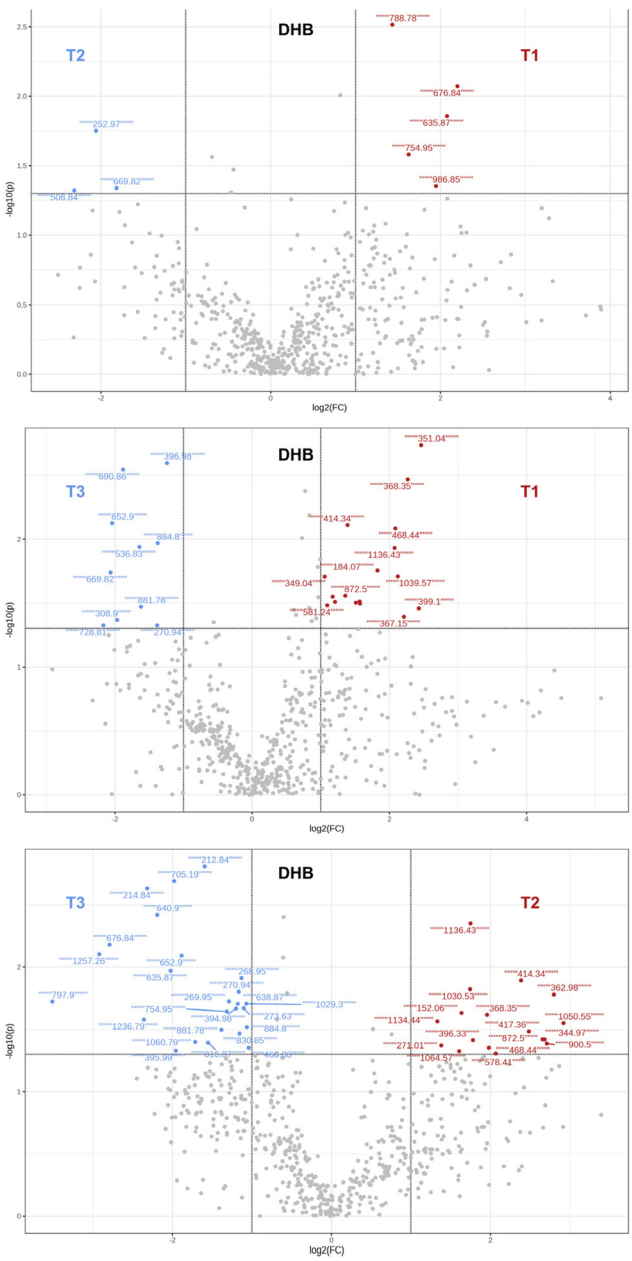

Fig. 4 Volcano plots showing significantly up- and downregulated spectral features (DHB matrix) for treatment comparisons T1 *vs.* T2 (top panel), T1 *vs.* T3 (middle panel), and T2 *vs.* T3 (bottom panel). A total of 8, 27, and 42 regulated species were identified for T1 *vs.* T2, T1 *vs.* T3, and T2 *vs.* T3 treatment pairs, respectively.

volcano plot that aims to capture the spectral features with both biological and statistical significance by setting cutoff thresholds for the peak intensity fold change (FC = 2) and the p values (p = 0.05) of the two-sample t-test, respectively.[20] Selecting for both biological significance (FC > 2) and statistical significance (p < 0.05) enabled pairwise comparisons between the three treatments (three replicates for each) (see Fig. 3 for the CHCA matrix, and Fig. 4 for DHB). The applied cutoff values aimed to strike the balance between statistical significance and the effect size. In Fig. 3, the pairwise comparison of T1 and T2 treatments (top panel) showed only three significantly regulated species indicating a probable similarity

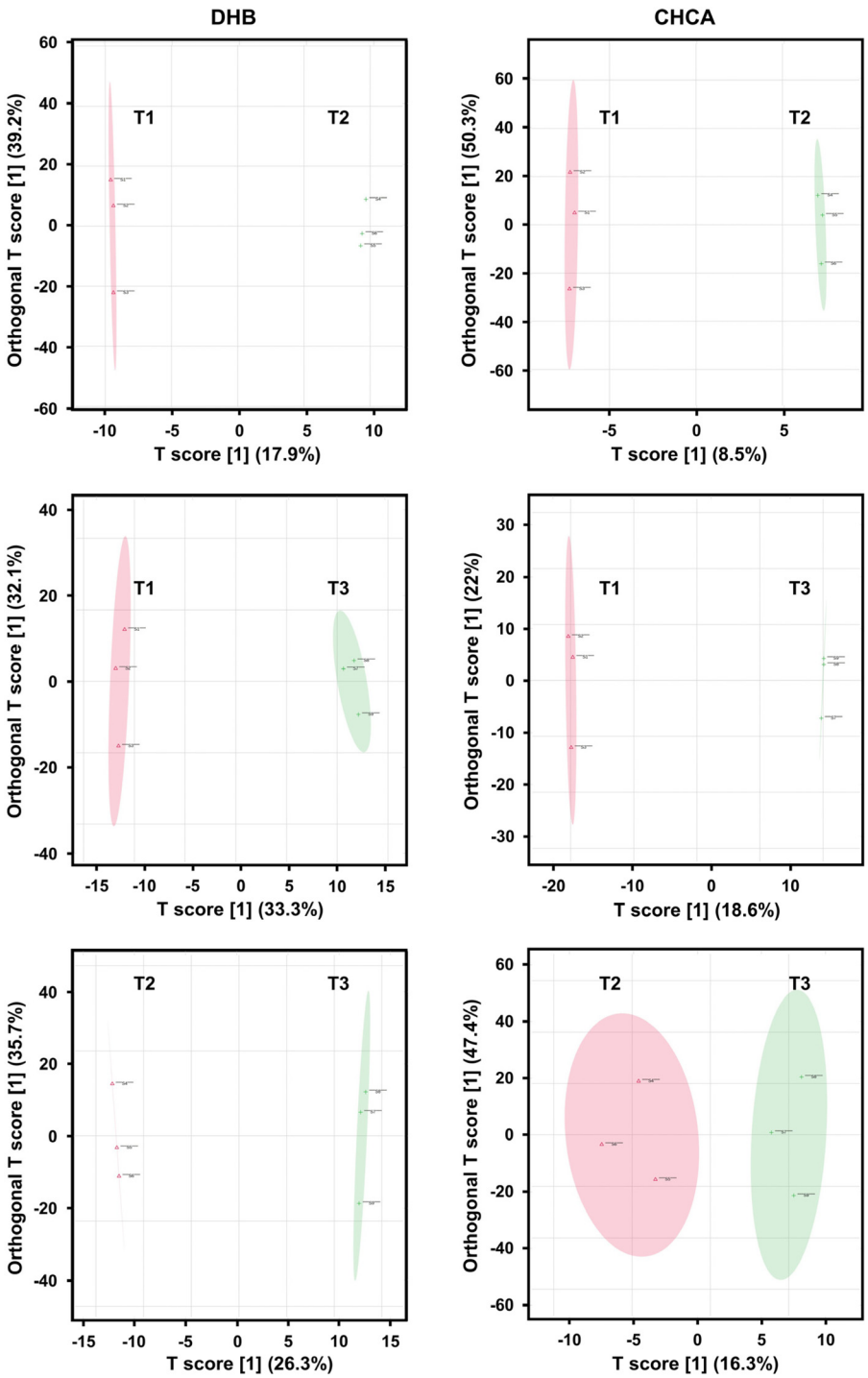

Fig. 5 Score plots for OPLS-DA of MALDI-MS spectra separate samples according to their treatments using both DHB (left panels) and CHCA (right panels) matrices.

between these protocols. Comparison of T1 to T3 (middle panel) and T2 to T3 (bottom panel), however, showed substantial differences, resulting in 20 and 14 significantly regulated species. For example, ion abundances at m/z 568.14 (FC = 4.6 and p = 0.02), potentially corresponding to protonated $(Hex)_1(NeuGc)_1(Phos)_1$ ($\Delta m/z$ = 9 mDa), and at m/z 393.09 (FC = 2.1 and p = 0.01) potentially corresponding to protonated $(Hex)_1(Pent)_1(Phos)_1$ ($\Delta m/z$ = 7 mDa), were upregulated for T1 treatment compared to T3. Additional eight spectral features at m/z 152.06, m/z 379.09, m/z 381.10, m/z 417.05, m/z 419.07, m/z 525.18, m/z 581.24, and m/z 637.31 indicated significant upregulation in both the T1 and T2 treatments compared to T3. Although no potential glycan structures were predicted for these species by the GlycoMod tool, they still might be associated with glycans or belong to a different group of metabolites that are indicative of treatment-related changes. Additional experiments, in particular tandem MS, might allow for the determination of their structure.

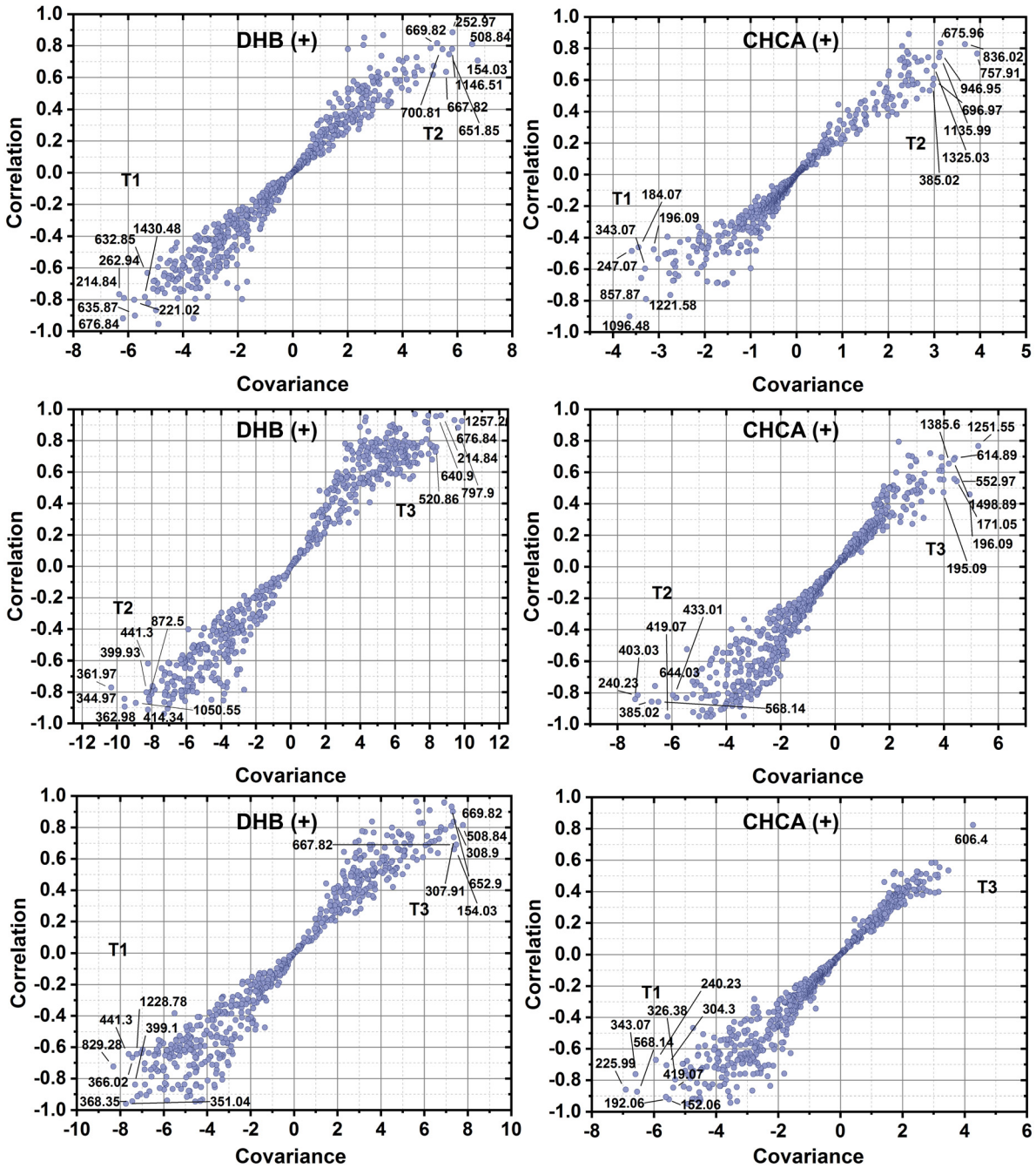

Fig. 6 *S*-plots produced by OPLS-DA models to explore spectral features most influential in distinguishing between treatment categories.

Like for the other matrix, using DHB for the comparison of the T1 and T2 treatments, only a few (a total of eight) significantly regulated species were observed (see the top panel in Fig. 4). Nevertheless, comparing treatments T1 and T2 to T3 major differences were observed resulting in 27 (middle panel in Fig. 4) and 42 (bottom panel in Fig. 4) significantly regulated species, respectively. Two of the regulated species in the T2 to T3 comparison, *m*/*z* 705.19 (FC = 0.3 and p = 0.002) and *m*/*z* 1029.30 (FC = 0.5 and p = 0.02), potentially correspond to potassiated oligohexoses, $(Hex)_4$ ($\Delta m/z$ = 5 mDa) and $(Hex)_6$ ($\Delta m/z$ = 9 mDa), respectively. Comparing treatments T1 and T2 to T3 (middle and bottom panels in Fig. 4), seven species, at *m*/*z* 368.35, *m*/*z* 414.34, *m*/*z* 468.44, *m*/*z* 872.50, *m*/*z* 900.5, *m*/*z* 1050.55, and *m*/*z* 1136.43, were upregulated in both cases, whereas three species, at *m*/*z* 270.94, *m*/*z* 881.78, and *m*/*z* 884.80, were downregulated.

To find the spectral features that account for most of the differences between the spectra, multivariate statistical analysis was carried out by OPLS-DA. The rationale behind choosing OPLS-DA lies in the ability of this supervised model to identify variables that account for most of the differences between spectra from predefined sample groups. In contrast, unsupervised Principal Component Analysis (PCA) often fails to demonstrate the separation between sample groups due to significant within-group variations.[21] Score plots generated by OPLS-DA for the pairwise treatment comparisons with different matrices (see Fig. 5) demonstrated clear distinctions between samples using both DHB (left panels) and CHCA (right panels) matrices. *S*-plots based on the OPLS-DA models were generated to identify the spectral features that are most responsible for the separation between treatment groups. The *S*-plots in Fig. 6 display the covariance, p[1], on the x-axis as a measure of the influence of each spectral feature on the separation of treatments, and the correlation, p(corr)[1], on the y-axis that represents the reliability of the contribution of a spectral feature to the model. In Fig. 6, the ionic species that appear in the wings of the *S*-plots are both influential and reliable in the treatment separation. Potentially they can be used as biomarkers for treatment discrimination.

Finally, VIP scores, which provide a quantitative measure of the discriminative power of each feature, were determined to rank the detected ionic species in the order of their influence on the model (see Fig. 7). The top 20 spectral features with high VIP scores (VIP > 1.5) are shown for the three pairwise treatment comparisons in Fig. 7. The top and bottom panels correspond to CHCA and DHB matrices, respectively. In T2 *vs.* T3 and T1 *vs.* T3 comparisons using CHCA matrix, ten common spectral features highlighted in green received VIP scores > 1.95 and they were found to be highly abundant in T1 and T2 samples. For the spectra obtained with DHB matrix,

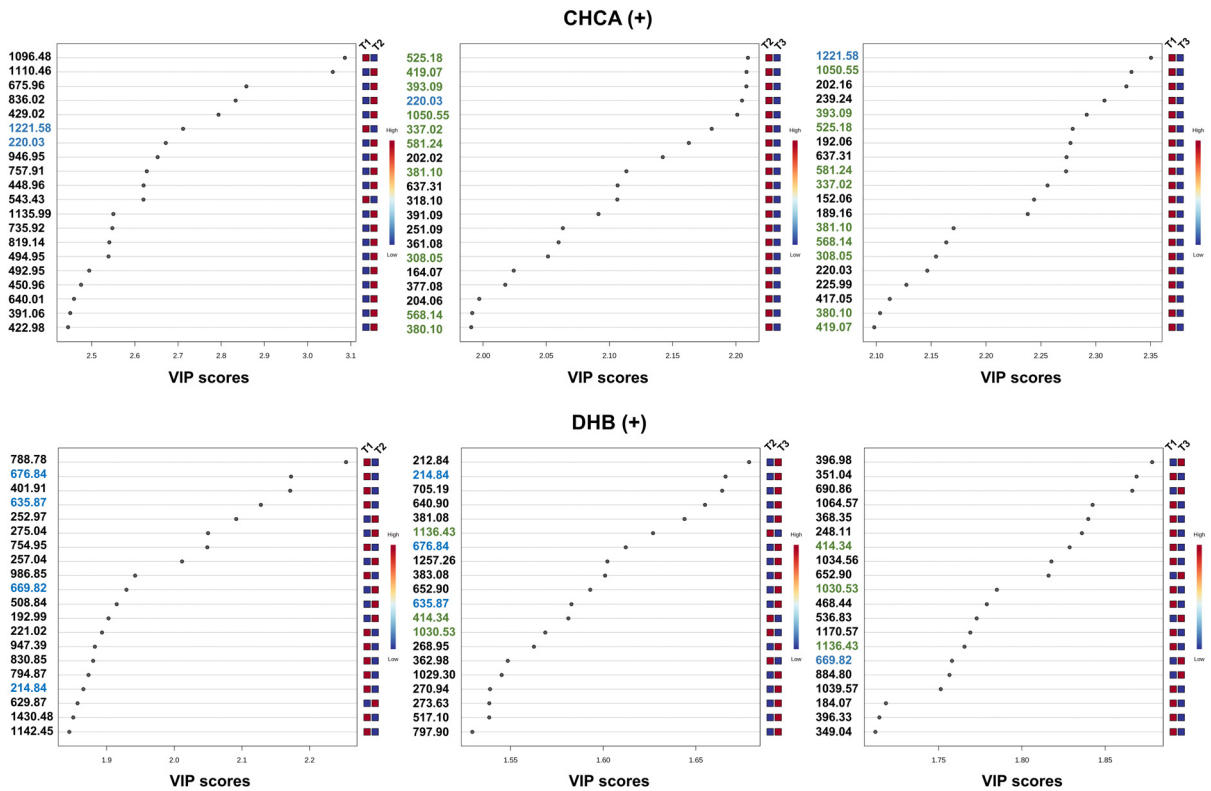

Fig. 7 VIP scores plots depicting 20 ionic species (VIP > 1.5) with most significant contributions to separating treatments T1, T2, and T3 in OPLS-DA models. Common spectral features observed between pairwise comparisons are indicated with their *m*/*z* values in color (blue and green).

relatively lower VIP scores were observed for the common features.

Conclusions

The types and abundances of FNGs and other metabolites in tomato xylem sap were considered as early indicators of nutrient deficiency in developing plants. Detection of oligosaccharides, including FNGs, and other small molecules from the resuspended lyophilate of tomato xylem sap was performed using high performance MS with MALDI ionization. The analyzed xylem sap originated from plants treated according to three growth protocols with different types of supplied nutrients. Treatment T1 was used as a control without any nutrient supplementation, relying only on the naturally accessible N, P, and K in the soil. The "ideal" supplementation was treatment T2, which provided all the N, P, and K required by the plants in the form of fertilizers, whereas nitrogen deficient growth conditions were established for treatment T3. The acquired spectra reflected the resulting metabolite compositions, including the abundances of plant complex type FNGs. Comparative univariate and multivariate statistical analysis by volcano plots and OPLS-DA, respectively, were used to evaluate the differences between spectra recorded for the control and the two treatment types. Comparison of the spectral features for the treatments demonstrated significant differences in the abundances of some chemical species, including some FNGs. Many of these statistically significant abundance ratios and fold changes were over fivefold. These included both FNGs and non-FNG compounds that can be considered as early indicators of nutrient deficiency. Our results reveal that the potential nutrient deficiency indicators can be expanded to other metabolites beyond FNGs. To gain a deeper understanding of how changes in metabolic pathways and the abundances of associated species are linked to growth, and to illustrate how plants prioritize responses to conflicting stimuli, future studies can explore the impact of nutrients and lights conditions. As the m/z values of detected FNGs are larger than m/z 1800, selecting a wider m/z range for the next group of samples is recommended. In addition, incorporating tandem MS will provide structural information and enhance confidence in the identification of chemical species.

Author contributions

Conceptualization of the project was initiated by I. K., D. A. L., and A. V., and the funding was secured by I. K. The research methodology was established by Z. S., I. V., I. K., M. D., and A. V. The investigations and the data curation were carried out by I. K. and M. D. Formal analysis, validation, and visualization of the data were carried out by M. D. and A. V. The original draft was written by M. D., and reviewed and edited by A. V., D. A. L., and I. K.

Conflicts of interest

The authors declare no conflict of interest related to this project.

Acknowledgements

This work was supported by the Ministry of Culture and Innovation of Hungary. Project No. 2021-1.2.4-TÉT-2021-00048 has been implemented with the support provided by the National Research, Development, and Innovation Fund, financed under the 2021-1.2.4-TÉT funding scheme. The authors are grateful for the financial support.

References

1 Y. J. Zheng, Z. Q. Yang, J. Luo, Y. Zhang, N. Jiang and W. A. Khattak, *Front. Plant Sci.*, 2023, **14**, 1197553.
2 D. A. A. Martinez, U. E. E. Loening, M. C. C. Graham and A. Gathorne-Hardy, *Front. Sustain. Food Syst.*, 2021, **5**, 701310.
3 D. H. Suh, Y. X. Kim, E. S. Jung, S. Lee, J. Park, C. H. Lee and J. Sung, *Molecules*, 2020, **25**, 4714.
4 S. Graeff, D. Steffens and S. Schubert, *J. Plant Nutr. Soil Sci.*, 2001, **164**, 445–450.
5 A. Amtmann and P. Armengaud, *Curr. Opin. Plant Biol.*, 2009, **12**, 275–283.
6 L. Z. Samarah, T. H. Tran, G. Stacey and A. Vertes, *Anal. Chem.*, 2020, **92**, 7299–7306.
7 H. Hirayama, *Trends Glycosci. Glycotechnol.*, 2018, **30**, E161–E167.
8 M. Maeda and Y. Kimura, *Front. Plant Sci.*, 2014, **5**, 429.
9 M. Katsube, N. Ebara, M. Maeda and Y. Kimura, *Front. Plant Sci.*, 2021, **11**, 610124.
10 R. Strasser, *Glycobiology*, 2016, **26**, 926–939.
11 B. Mátyás, J. Singer, M. Szarka, D. A. Lowy, B. Dönczo, P. Makleit, V. E. Failoc-Rojas, A. Ramirez, P. Martínez, Z. Sándor, I. Kincses and A. Guttman, *Electrophoresis*, 2021, **42**, 200–205.
12 T. De Coninck, K. Gistelinck, H. J. C. van Rensburg, W. van den Ende and E. J. M. Van Damme, *Biomolecules*, 2021, **11**, 756.
13 H. Kaulfürst-Soboll, M. Mertens-Beer, R. Brehler, M. Albert and A. von Schaewen, *Front. Plant Sci.*, 2021, **12**, 635962.
14 R. Strasser, *Front. Plant Sci.*, 2022, **13**, 897549.
15 B. Priem, R. Gitti, C. A. Bush and K. C. Gross, *Plant Physiol.*, 1993, **102**, 445–458.
16 B. Mátyás, J. Singer, M. Szarka, D. A. Lowy, B. Dönczo, P. Makleit, V. E. Failoc-Rojas, A. Ramirez, P. Martínez, Z. Sándor, I. Kincses and A. Guttman, *Electrophoresis*, 2021, **42**, 800–800.

17 I. Kincses, J. R. Melendez, L. Ramirez-Cando, D. Burbano-Salas, D. Lowy, G. Cuenca Nevarez, V. Talledo Solorzano, J. Morales Arteaga, B. Mendoza and Z. Sandor, *F1000Research*, 2020, **9**, 781.
18 Y. Tsujimori, M. Ogura, M. Z. Rahman, M. Maeda and Y. Kimura, *Biosci., Biotechnol., Biochem.*, 2019, **83**, 1310–1314.
19 C. A. Cooper, E. Gasteiger and N. H. Packer, *Proteomics*, 2001, **1**, 340–349.
20 M. Ebrahimpoor and J. J. Goeman, *Briefings Bioinf.*, 2021, **22**, bbab053.
21 B. Shrestha, J. M. Patt and A. Vertes, *Anal. Chem.*, 2011, **83**, 2947–2955.
22 H. Egner, H. Riehm and W. R. Domingo, *Kungl. Lantbrukshogskolans Ann.*, 1960, **26**, 199–215.
23 I. Jaszberenyi, J. Loch and J. Sarkadi, *Commun. Soil Sci. Plant Anal.*, 1994, **25**, 1771–1777.
24 V. J. G. Houba, I. Novozamsky and E. Temminghoff, *Soil and plant analysis, Department of Soil Science and Plant Nutrition*, Wageningen Agricultural University, Wageningen, The Netherlands, 1994, vol. 5, pp. 12–22.